

Fast Magnetic Resonance Electrical Impedance Tomography with highly undersampled data

Y. Song and H. Ammari and J.K. Seo

Research Report No. 2016-17
March 2016

Seminar für Angewandte Mathematik
Eidgenössische Technische Hochschule
CH-8092 Zürich
Switzerland

FAST MAGNETIC RESONANCE ELECTRICAL IMPEDANCE TOMOGRAPHY WITH HIGHLY UNDERSAMPLED DATA *

YIZHUANG SONG [†], HABIB AMMARI [‡], AND JIN KEUN SEO [§]

Abstract. This paper describes the mathematical grounds for a highly undersampled Magnetic Resonance Electrical Impedance Tomography (MREIT) method, with the aim of visualizing the dynamic changes in electrical tissue properties that occur in response to physiological activity. MREIT with fully sampled MR data (satisfying the Nyquist criterion) has been shown to be capable of high-resolution conductivity imaging in numerical simulations and in animal experiments. However, when the data are undersampled (violating the Nyquist criterion for reducing data acquisition time), it is difficult to extract the component of magnetic flux density that is induced by boundary injection currents, and it is the data from this component that are used in performing the standard MREIT algorithm. Here, we show that it is possible to localize small conductivity perturbations using highly undersampled MR data. We perform various numerical simulations to support our theoretical results.

Key words. MREIT, MRI, Inverse problem

AMS subject classifications. 35R30, 35J61, 35Q61

1. Introduction. Magnetic resonance electrical impedance tomography (MREIT) is a recently developed MR-based imaging method that enables high-spatial-resolution imaging of electrical conductivity distribution at a frequency below a few kHz [18, 19, 26]. The spatial contrast information gained in this manner appears to be unique as no other method, including electrical impedance tomography (EIT), has managed to produce high-resolution conductivity images in realistic environments. The drawback of MREIT is its low temporal resolution due to the slow data acquisition process, which is unavoidable because of the constraints of imaging obtained using an MR scanner; i.e., the MR data acquisition time is roughly proportional to the number of time-consuming phase-encoding steps in k-space (or the spatial frequency domain)[21]. Although EIT enables data acquisition with high temporal resolution, when its inherent ill-posed nature is taken into consideration, it is difficult to probe small local conductivity changes located away from the measuring positions.

The aim of this study was to develop a highly undersampled MREIT method for visualizing the dynamic changes in electrical tissue properties that result from tissue physiological activity[4, 5, 7, 10, 15, 25]. The poor temporal resolution of MREIT can be greatly improved by using highly undersampled MRI data that skip many phase encoding lines in the k-space, given the inherent tradeoff between spatial and temporal resolutions. Accordingly, when undersampled k-space data are used, it will be necessary to incorporate some prior information regarding the target image.

Some difficulties arise in using highly undersampled MR data for MREIT reconstruction. In standard MREIT reconstruction, it is necessary to measure the

*Song was supported by National Science Foundation of China (Grant No. 11501336, 11426147), the Research Fund for Excellent Young and Middle aged Scientists of Shandong Province (No. BS2014SF020) and the Scientific Research Foundation for the Returned Overseas Chinese Scholars, State Education Ministry. Seo was supported by the National Research Foundation of Korea (NRF) grant 2015R1A5A1009350.

[†]School of Mathematical Sciences, Shandong Normal University, Jinan, 250014, P. R. China.

[‡]Department of Mathematics, ETH Zürich, Rämistrasse 101, CH-8092 Zürich, Switzerland (habib.ammari@math.ethz.ch).

[§]To whom correspondence should be addressed (seoj@yonsei.ac.kr). Department of Computational Science and Engineering, Yonsei University, Seoul, 120-749, Korea.

z -component of magnetic flux density (B_z) induced by an external current injected through surface electrodes, where the z -axis is assumed to be in the same direction as the main magnetic field of the scanner. MREIT reconstruction is based on the fact that B_z reflects the conductivity distribution σ inside the imaging object Ω via Ampère's law $\nabla \times \mathbf{B} \propto \sigma \mathbf{E}$, where \mathbf{E} is the corresponding electrical field. The B_z data can be extracted from the inverse Fourier transform of fully sampled k -space MR data given by

$$S(k_x, k_y, z_0) = \int_{\Omega \cap \{z=z_0\}} M(x, y, z) e^{icB_z(x, y, z_0)} e^{i2\pi(k_x x + k_y y)} dx dy,$$

where $M(x, y, z)$ is a conventional MR magnitude image and c is a known constant. Here, any systematic phase artifacts were ignored. However, B_z cannot be extracted from a highly undersampled MRI data. The undersampled k -space data are obtained by skipping the data of the time-consuming phase-encoding direction (e.g. y -direction) by the factor of N . In accordance with the Poisson summation formula [21], only N -folded data of $M e^{icB_z}$ are obtained as a nonlinear function of B_z . It is impossible to extract B_z for the folded data, and it is difficult to handle the inverse problem of conductivity imaging using the N -folded data of $M e^{icB_z}$ alone. A careful analysis is necessary to express conductivity in terms of the undersampled MR data.

In this paper, we show that it is possible to use highly undersampled data to localize conductivity changes in time, under the assumption that the time-difference conductivity is sparsely supported within an imaging object. We find that the time derivative from the N -folded data of $M e^{icB_z}$ provides location information for conductivity changes by using an asymptotic expansion of the time derivative of B_z , in which the magnitude decays quadratically with distance from the support. We perform various numerical simulations to test the feasibility of the proposed method.

2. Basic imaging setup of undersampled MREIT. Let the imaging object such as human body occupy a three-dimensional domain $\Omega \subset \mathbb{R}^3$ with a smooth connected boundary $\partial\Omega$. Assume that $\sigma(\mathbf{r}, t)$ is an isotropic conductivity depending on position $\mathbf{r} = (x, y, z) \in \Omega$ and time t . The goal is to detect the time differential of the conductivity, $\frac{\partial\sigma}{\partial t}$, using MREIT technique with a highly undersampled MR data violating Nyquist criteria [21].

Let us begin with briefly reviewing the process of data acquisition [16, 17] in MREIT to explain difficulties of extracting the data from a highly undersampled k -space data. Let the direction of the main magnetic field of MRI scanner be the z -axis. In MREIT, we attach a pair of surface electrodes \mathcal{E}^+ and \mathcal{E}^- on $\partial\Omega$ to inject a current of I mA with the pulse width of T_c during the MR data collection process, as shown in Figure 2.1. The injection current produces the internal electrical field ($\mathbf{E} = (E_x, E_y, E_z)$), current density ($\mathbf{J} = (J_x, J_y, J_z)$) and magnetic flux density ($\mathbf{B} = (B_x, B_y, B_z)$) inside Ω . The z -component of \mathbf{B} , B_z , produces an extra phase shift in the MR signal which can be described as follows: For each slice $\Omega_{z_0} := \Omega \cap \{z = z_0\}$, the k -space MR signals influenced by B_z can be expressed as

$$S(k_x, k_y, z_0, t) = \int_{\Omega_{z_0}} M(x, y, z_0) e^{i\gamma T_c B_z(x, y, z_0, t)} e^{i2\pi(k_x x + k_y y)} dx dy, \quad (2.1)$$

where $M(x, y, z) > 0$ is a conventional MR magnitude image and $\gamma = 26.75 \times 10^7$ rad/T·s, the gyromagnetic ratio of hydrogen. Here, all systematic phase artifacts were ignored.

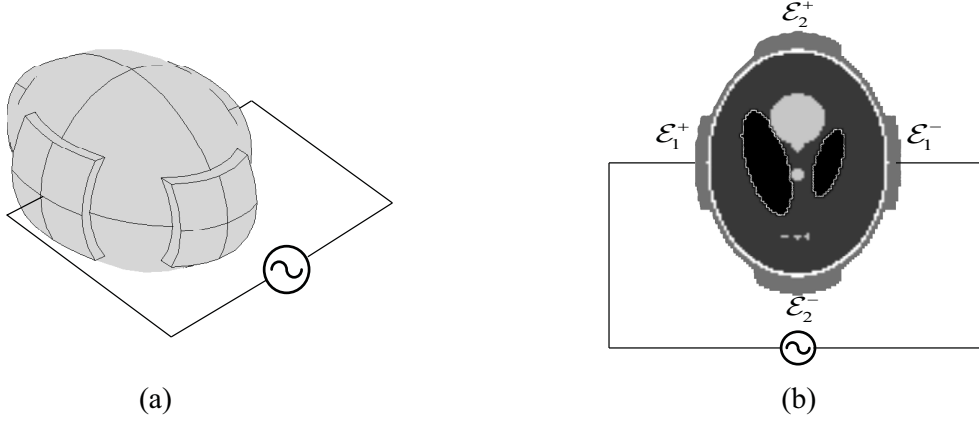


FIG. 2.1. A current is injected to the imaging object Ω through a pair of electrodes attached on $\partial\Omega$. (a) The imaging object with electrodes attached on its boundary. (b) The cross-sectional image of Ω with the electrode configuration.

In MRI, the spacial resolution of M is determined by the k-space sampling. Assume that we apply the phase encoding gradient in y -direction and the frequency encoding gradient in x -direction. Assume that the MR image M is displayed in the region $\{(x, y) : -\frac{FOV}{2} < x, y < \frac{FOV}{2}\}$ with the pixel width $\Delta x = \Delta y$, where FOV denotes the field-of-view. According to the Nyquist sampling theorem [21], this image resolution corresponds to the k-space sampling distance $\Delta k_x = \Delta k_y = 1/FOV$ and the maximum spatial frequency being $1/\Delta x$. For simplicity, assume $FOV = 1$. In the absence of the injection current, the discrete image of M , $\frac{FOV}{\Delta x} \times \frac{FOV}{\Delta x}$ image matrix, can be obtained by the inverse discrete Fourier transform with the fully sampled k-space data

$$\{S(m\Delta k_x, n\Delta k_y, z_0, t) : m, n = 0, \pm 1, \dots, \pm \frac{1}{2\Delta y}\}.$$

The data acquisition speed is roughly proportional to $\frac{1}{2\Delta k_y}$ in the time-consuming phase encoding direction (y -direction). For fast MREIT, we reduce the scan-time significantly by using N -times undersampled k-space data

$$\{S(m\Delta k_x, jN\Delta k_y, z_0, t) : m = 0, \pm 1, \dots, \pm \frac{1}{2\Delta y}, j = 0, \pm 1, \dots, \pm \frac{1}{2N\Delta y}\}.$$

From the Poisson summation formula [21], the inverse Fourier transform of N -times undersampled k-space data in (2.1) produces the following N -folded image:

$$\mathcal{M}^N(x, y, z_0, t) := \sum_{j=0}^{N-1} M(x, y + \frac{j}{N}, z_0) e^{i\gamma T_c B_z(x, y + \frac{j}{N}, z_0, t)}. \quad (2.2)$$

All reconstruction methods in MREIT use the full sampling k-space data which is the case of $N = 1$. In this case, the B_z data is extracted easily from \mathcal{M}^1 from the identity (2.2), because the imaginary part of $\frac{1}{\gamma T_c} \ln\left(\frac{\mathcal{M}^1}{M}\right)$ directly gives a wrapped B_z data. With this B_z data, MREIT methods [18, 19, 20, 22, 23, 26] reconstruct the

conductivity σ using the Biot-Savart law:

$$\frac{1}{\mu_0} B_z(\mathbf{r}, t) = \int_{\Omega} \frac{(\mathbf{r} - \mathbf{r}') \times (\sigma(\mathbf{r}', t) \nabla u(\mathbf{r}', t))}{4\pi |\mathbf{r} - \mathbf{r}'|} \cdot \mathbf{e}_z d\mathbf{r}' + \frac{1}{\mu_0} \mathcal{H}(\mathbf{r}) \quad \text{for } \mathbf{r} \in \Omega, \quad (2.3)$$

where $\mathbf{e}_z = (0, 0, 1)$, $\mu_0 = 4\pi \times 10^{-7} \text{H/m}$ is the permeability of the free space and \mathcal{H} is a harmonic function in Ω , representing the z -component of the magnetic field induced by the current flux density on electrodes and lead wires [23]. Here, $u(\mathbf{r}, t)$ satisfies

$$\begin{cases} \nabla \cdot (\sigma(\mathbf{r}, t) \nabla u(\mathbf{r}, t)) = 0 & \text{for } \mathbf{r} \in \Omega, \\ -\sigma(\mathbf{r}, t) \frac{\partial u}{\partial \mathbf{n}}(\mathbf{r}, t) = g(\mathbf{r}) & \text{for } \mathbf{r} \in \partial\Omega, \end{cases} \quad (2.4)$$

where $g \in L^2_{\diamond}(\partial\Omega) = \{\psi \in L^2(\partial\Omega) : \int_{\partial\Omega} \psi ds = 0\}$ represents the injection current through the pair of the surface electrodes, \mathbf{n} denotes the unit outer normal vector to $\partial\Omega$.

However, with undersampled k-space data \mathcal{M}^N ($N \geq 2$), it may not be possible to extract B_z from the formula (2.2). Let us see this non-uniqueness for the case of $N = 3$. It is easy to see that there are infinitely many ϕ such that

$$0 = \sum_{j=0}^2 \mathcal{M}^1(x, y + \frac{j}{3}, z_0) \left(1 - e^{i\gamma T_c \phi(x, y + \frac{j}{3})}\right) \quad \text{for } (x, y, z_0) \in \Omega_{z_0}.$$

Then, if B_z satisfies (2.2), so does for $B_z + \phi$. This non-uniqueness with the nonlinear relation between B_z and \mathcal{M}^N is the major difficulty to deal with the inverse problem corresponding to the undersampled MREIT.

3. Main results. In this section, we show feasibility of the undersampled MREIT in recovering $\frac{\partial \sigma}{\partial t}$ under its sparsity constraint. We assume that $\sigma(\mathbf{r}, t)$ is of the following form:

$$\sigma(\mathbf{r}, t) = \sigma(\mathbf{r}, 0) + \eta(t) \chi_D(\mathbf{r}) \quad \text{for } \mathbf{r} \in \Omega, \quad t > 0,$$

where D is a smooth subdomain of Ω , χ_D is the characteristic function of D , and η is a C^1 function such that $\eta'(t) \neq 0$ and $\eta(0) = 0$. We also assume that there exists a positive constant Λ such that

$$\frac{1}{\Lambda} \leq \sigma(\mathbf{r}, t) \leq \Lambda \quad \text{for } \mathbf{r} \in \Omega \quad \text{and } t > 0. \quad (3.1)$$

Denote $D_{z_0} = \Omega_{z_0} \cap D$. Assume that M in (2.1) satisfies

$$\frac{1}{c} \leq M(x, y, z_0) \leq c \quad \text{for } (x, y, z_0) \in \Omega_{z_0}, \quad (3.2)$$

where c is a positive constant. Assume that we have the reference data \mathcal{M}^1 at time $t = 0$, which is obtained from a fully sampled k-space data at a fixed time period. Let $N \geq 2$. The goal is to detect D_{z_0} from the N -folded data \mathcal{M}^N for $t > 0$.

Taking the time derivative on (2.2), we obtain

$$\frac{\partial \mathcal{M}^N}{\partial t}(x, y, z_0, t) = \sum_{j=0}^{N-1} \mathcal{M}^1(x, y + \frac{j}{N}, z_0) \frac{\partial B_z}{\partial t}(x, y + \frac{j}{N}, z_0, t). \quad (3.3)$$

Let us introduce a function \mathcal{B}^N defined by:

$$\mathcal{B}^N(x, y, z_0, t) = \frac{1}{i\gamma T_c} \frac{\frac{\partial}{\partial t} \mathcal{M}^N(x, y, z_0, t)}{\mathcal{M}^1(x, y, z_0, 0)} \quad \text{for } (x, y, z_0) \in \Omega_{z_0}. \quad (3.4)$$

Note that \mathcal{B}^1 , in the special case when $N = 1$, is a wrapped version of $\frac{\partial B_z}{\partial t}$. We will explain how the data \mathcal{B}^N probes

$$D_{z_0}^N = \{(x, y, z_0) \in \Omega_{z_0} : (x, y - \frac{j}{N}, z_0) \in D_{z_0}, j = 0, 1, \dots, N-1\}.$$

In the next section, we provide a rigorous analysis for the simple case of D .

3.1. Estimation of the folded domain $D_{z_0}^N$. For a rigorous analysis, let us restrict ourselves to the simplest case where $\sigma(\mathbf{r}, 0) \equiv 1$ for $\mathbf{r} \in \Omega$ and D is a simply connected domain. To be precise, D is expressed as

$$D = \mathbf{r}_0 + \epsilon \widehat{D},$$

where \widehat{D} is a smooth domain containing the origin, $\epsilon > 0$ is a small scaling factor, and $\mathbf{r}_0 = (x_0, y_0, z_0) \in D_{z_0}$. We also assume that $L := \text{dist}(D, \partial\Omega) > 0$. For each $t > 0$, let $\mathbf{v}(\cdot, t) \in H_{loc}^1(\mathbb{R}^3)$ be a function solving the equation

$$\begin{cases} \Delta \mathbf{v} = 0 & \text{in } \mathbb{R}^3 \setminus \widehat{D}, \\ \Delta \mathbf{v} = 0 & \text{in } \widehat{D}, \\ \mathbf{v}^+ - \mathbf{v}^- = 0 & \text{on } \partial \widehat{D}, \\ (1 + \eta(t)) \frac{\partial \mathbf{v}^+}{\partial \mathbf{n}} - \frac{\partial \mathbf{v}^-}{\partial \mathbf{n}} = 0 & \text{on } \partial \widehat{D}, \\ \mathbf{v}(\xi) - \xi \rightarrow 0 & \text{as } |\xi| \rightarrow +\infty, \end{cases} \quad (3.5)$$

where $\xi = \frac{\mathbf{r} - \mathbf{r}_0}{\epsilon}$ is a local variable, $\mathbf{v}^+ = \mathbf{v}|_{\widehat{D}}$ and $\mathbf{v}^- = \mathbf{v}|_{\Omega \setminus \widehat{D}}$. Let $\Phi(\mathbf{r}) = -\frac{1}{4\pi|\mathbf{r}|}$ be the fundamental solution. We introduce

$$\begin{aligned} \Gamma_{\widehat{D}}^1(\xi, t) &= \mathcal{S}_{\widehat{D}}[\nabla_{\xi}^{\perp} \mathbf{v}(\xi, t) \mathbf{n}](\xi), \\ \Gamma_{\widehat{D}}^2(\xi, t) &= \mathcal{S}_{\widehat{D}} \left[\nabla \mathcal{S}_{\widehat{D}} \left[\nabla_{\xi}^{\perp} \frac{\partial}{\partial t} (\eta(t) \mathbf{v}(\xi, t)) \nabla u(\mathbf{r}_0, 0) \cdot \mathbf{n} \right] \cdot \mathbf{n} \right] (\xi), \end{aligned}$$

where $u(\mathbf{r}, t)$ is the solution of (2.4) with the homogeneous reference conductivity $\sigma(\mathbf{r}, 0) \equiv 1$ for $\mathbf{r} \in \Omega$ and $\mathcal{S}_{\Omega}[\psi]$ is the single layer potential defined by

$$\mathcal{S}_{\Omega}[\psi](\mathbf{r}) = \int_{\partial\Omega} \Phi(\mathbf{r} - \mathbf{r}') \psi(\mathbf{r}') dS_{\mathbf{r}'} \quad \text{for } \mathbf{r} \in \mathbb{R}^3 \setminus \partial\Omega.$$

Let $D_d = \{\mathbf{r} \in \Omega : \text{dist}(\mathbf{r}, D) < d\}$ for a fixed positive number d satisfying

$$\sqrt{\epsilon} < d < \frac{\text{diam}(\Omega_{z_0})}{3N}. \quad (3.6)$$

Now, we are ready to state our main theorem, which allows to detect N -folded $D_{z_0}^N$ from a simple thresholding.

THEOREM 3.1. *Assume that d satisfies the condition (3.6).*

(i) If $\mathbf{r} \in D_{z_0}^N$, then

$$\begin{aligned} \frac{1}{\mu_0} \mathcal{B}^N(\mathbf{r}, t) &= \frac{1}{i\gamma T_c} \frac{\mathcal{M}^1(\mathbf{r}_\sharp, t)}{\mathcal{M}^1(\mathbf{r}, 0)} \nabla u(\mathbf{r}_0, 0) \\ &\quad \left[-\eta'(t) \Gamma_{\bar{D}}^1 \left(\frac{\mathbf{r}_\sharp - \mathbf{r}_0}{\epsilon}, t \right) + \eta(t) \Gamma_{\bar{D}}^2 \left(\frac{\mathbf{r}_\sharp - \mathbf{r}_0}{\epsilon}, t \right) \right] \epsilon + O(\epsilon^3), \end{aligned} \quad (3.7)$$

where \mathbf{r}_\sharp is the point in D_{z_0} such that $\mathbf{r}_\sharp - \mathbf{r} = (0, \frac{n}{N}, 0)$ for some integer n .

(ii) There exists a positive constant C independent of ϵ such that

$$\left| \frac{1}{\mu_0} \mathcal{B}^N(\mathbf{r}, t) \right| \leq C \epsilon^3, \quad (3.8)$$

for $\mathbf{r} \in (\Omega \setminus D_d) \cap \{z = z_0\}$.

The proof of Theorem 3.1 relies on the following Lemma, which provides an estimation of $\frac{\partial B_z}{\partial t}$ both inside and outside of D .

LEMMA 3.2. *Under the assumption of Theorem 3.1, we have the followings:*

(i) For $\mathbf{r} \in D$, we have

$$\frac{1}{\mu_0} \frac{\partial B_z}{\partial t}(\mathbf{r}, t) = \nabla u(\mathbf{r}_0, 0) \cdot \left[-\eta'(t) \Gamma_{\bar{D}}^1 \left(\frac{\mathbf{r} - \mathbf{r}_0}{\epsilon}, t \right) + \eta(t) \Gamma_{\bar{D}}^2 \left(\frac{\mathbf{r} - \mathbf{r}_0}{\epsilon}, t \right) \right] \epsilon + O(\epsilon^3).$$

(ii) For $\mathbf{r} \in \Omega \setminus D_d$, we have

$$\left| \frac{1}{\mu_0} \frac{\partial B_z}{\partial t}(\mathbf{r}, t) \right| \leq C \frac{\epsilon^3}{[d + \text{dist}(\mathbf{r}, D_d)]^2},$$

where C is a positive constant independent of ϵ .

Proof. (i) A simple integration by parts yields

$$u(\mathbf{r}, t) = -\eta(t) \int_D \nabla_{\mathbf{r}'} \Phi(\mathbf{r} - \mathbf{r}') \cdot \nabla u(\mathbf{r}', t) d\mathbf{r}' - \mathcal{D}_\Omega[f(\cdot, t)](\mathbf{r}) + \mathcal{S}_\Omega[g](\mathbf{r}) \quad \mathbf{r} \in \Omega, \quad (3.9)$$

where $f(\cdot, t) = u(\cdot, t)|_{\partial\Omega}$ and $\mathcal{D}_\Omega[\psi]$ is the double layer potential of $\psi \in L^2(\partial\Omega)$ given by $\mathcal{D}_\Omega[\psi](\mathbf{r}) = \int_{\partial\Omega} \frac{\partial\Phi(\mathbf{r} - \mathbf{r}')}{\partial\mathbf{n}_{\mathbf{r}'}} \psi(\mathbf{r}') dS_{\mathbf{r}'}$ for $\mathbf{r} \in \mathbb{R}^3 \setminus \partial\Omega$. Taking the time derivative on both sides of the identity (3.9), we obtain

$$\begin{aligned} -\frac{\partial u}{\partial t}(\mathbf{r}, t) &= \int_D \nabla_{\mathbf{r}'} \Phi(\mathbf{r} - \mathbf{r}') \cdot \nabla_{\mathbf{r}'} \left[\eta'(t) u(\mathbf{r}', t) + \eta(t) \frac{\partial u}{\partial t}(\mathbf{r}', t) \right] d\mathbf{r}' \\ &\quad + \mathcal{D}_\Omega \left[\frac{\partial f}{\partial t}(\cdot, t) \right] (\mathbf{r}, t) \quad \text{for } \mathbf{r} \in \Omega. \end{aligned} \quad (3.10)$$

Denoting $\mathbf{J}(\mathbf{r}, t) = -\sigma(\mathbf{r}, t) \nabla u(\mathbf{r}, t)$, we have

$$\frac{\partial \mathbf{J}}{\partial t}(\mathbf{r}, t) = -\frac{\partial \sigma}{\partial t}(\mathbf{r}, t) \nabla u(\mathbf{r}, t) - \sigma(\mathbf{r}, t) \nabla \frac{\partial u}{\partial t}(\mathbf{r}, t). \quad (3.11)$$

Substituting $\sigma(\mathbf{r}, t) = 1 + \eta(t) \chi_D$ and (3.10) into (3.11), we get

$$\begin{aligned} \frac{\partial \mathbf{J}}{\partial t}(\mathbf{r}, t) &= [1 + \eta(t) \chi_D] \\ &\quad \nabla \int_D \nabla_{\mathbf{r}'} \Phi(\mathbf{r} - \mathbf{r}') \cdot \nabla_{\mathbf{r}'} \left[\eta'(t) u(\mathbf{r}', t) + \eta(t) \frac{\partial u}{\partial t}(\mathbf{r}', t) \right] d\mathbf{r}' \\ &\quad - \eta'(t) \nabla u(\mathbf{r}, t) \chi_D + [1 + \eta(t) \chi_D] \nabla \mathcal{D}_\Omega \left[\frac{\partial f(\cdot, t)}{\partial t} \right] (\mathbf{r}, t). \end{aligned} \quad (3.12)$$

From (2.3), $\frac{\partial B_z}{\partial t}$ is expressed as

$$\frac{\partial B_z}{\partial t}(\mathbf{r}, t) = -\mu_0 \int_{\Omega} \nabla_{\mathbf{r}'} \Phi(\mathbf{r} - \mathbf{r}') \times \frac{\partial}{\partial t} \mathbf{J}(\mathbf{r}', t) \cdot \mathbf{e}_z d\mathbf{r}'. \quad (3.13)$$

Substituting the identity (3.12) into (3.13) and denoting $\nabla^\perp = (\frac{\partial}{\partial y}, -\frac{\partial}{\partial x}, 0)$, we get

$$\frac{1}{\mu_0} \frac{\partial B_z}{\partial t}(\mathbf{r}, t) = \sum_{j=1}^3 \mathcal{I}_j(\mathbf{r}, t) + \sum_{j=1}^3 \mathcal{R}_j(\mathbf{r}, t) \quad \text{for } \mathbf{r} \in \Omega, \quad (3.14)$$

where

$$\begin{aligned} \mathcal{I}_1(\mathbf{r}, t) &:= -\eta'(t) \int_D \nabla_{\mathbf{r}'} \Phi(\mathbf{r} - \mathbf{r}') \cdot \nabla_{\mathbf{r}'}^\perp u(\mathbf{r}', t) d\mathbf{r}', \\ \mathcal{I}_2(\mathbf{r}, t) &:= \eta(t) \eta'(t) \int_D \nabla_{\mathbf{r}'} \Phi(\mathbf{r} - \mathbf{r}') \cdot \nabla_{\mathbf{r}'}^\perp \int_D \nabla_{\tilde{\mathbf{r}}} \Phi(\mathbf{r}' - \tilde{\mathbf{r}}) \cdot \nabla u(\tilde{\mathbf{r}}, t) d\tilde{\mathbf{r}} d\mathbf{r}', \\ \mathcal{I}_3(\mathbf{r}, t) &:= \eta^2(t) \int_D \nabla_{\mathbf{r}'} \Phi(\mathbf{r} - \mathbf{r}') \cdot \nabla_{\mathbf{r}'}^\perp \int_D \nabla_{\tilde{\mathbf{r}}} \Phi(\mathbf{r}' - \tilde{\mathbf{r}}) \cdot \nabla \frac{\partial u}{\partial t}(\tilde{\mathbf{r}}, t) d\tilde{\mathbf{r}} d\mathbf{r}', \\ \mathcal{R}_1(\mathbf{r}, t) &:= \eta'(t) \int_{\Omega} \nabla_{\mathbf{r}'} \Phi(\mathbf{r} - \mathbf{r}') \cdot \nabla_{\mathbf{r}'}^\perp \int_D \nabla_{\tilde{\mathbf{r}}} \Phi(\mathbf{r}' - \tilde{\mathbf{r}}) \cdot \nabla u(\tilde{\mathbf{r}}, t) d\tilde{\mathbf{r}} d\mathbf{r}', \\ \mathcal{R}_2(\mathbf{r}, t) &:= \eta(t) \int_{\Omega} \nabla_{\mathbf{r}'} \Phi(\mathbf{r} - \mathbf{r}') \cdot \nabla_{\mathbf{r}'}^\perp \int_D \nabla_{\tilde{\mathbf{r}}} \Phi(\mathbf{r}' - \tilde{\mathbf{r}}) \cdot \nabla \frac{\partial u}{\partial t}(\tilde{\mathbf{r}}, t) d\tilde{\mathbf{r}} d\mathbf{r}', \\ \mathcal{R}_3(\mathbf{r}, t) &:= \int_{\Omega} [1 + \eta(t) \chi_D] \nabla_{\mathbf{r}'} \Phi(\mathbf{r} - \mathbf{r}') \cdot \nabla^\perp \mathcal{D}_\Omega \left[\frac{\partial f(\cdot, t)}{\partial t} \right] (\mathbf{r}') d\mathbf{r}'. \end{aligned}$$

Now, we use the inner expansion in [1, 2, 3] to get the following pointwise expansion

$$u(\mathbf{r}, t) = u(\mathbf{r}_0, 0) + \epsilon \mathbf{v}(\xi, t) \cdot \nabla u(\mathbf{r}_0, 0) + O(\epsilon^2) \quad \text{for } \mathbf{r} \in \bar{D}, \quad (3.15)$$

where $\xi = \frac{\mathbf{r} - \mathbf{r}_0}{\epsilon}$. Hence, we have

$$\nabla u(\mathbf{r}, t) = \epsilon \nabla_{\mathbf{r}} \mathbf{v}(\xi, t) \nabla u(\mathbf{r}_0, 0) + O(\epsilon) \quad \text{for } \mathbf{r} \in \bar{D}$$

and

$$\nabla^\perp u(\mathbf{r}, t) = \nabla_\xi^\perp \mathbf{v}(\xi) \nabla u(\mathbf{r}_0, 0) + O(\epsilon) \quad \text{for } \mathbf{r} \in \bar{D}.$$

Substituting (3.14) into \mathcal{I}_j ($j = 1, 2, 3$), we obtain

$$\begin{aligned} \sum_{j=1}^3 \mathcal{I}_j(\mathbf{r}, t)(\mathbf{r}, t) &= -\eta'(t) \nabla u(\mathbf{r}_0, 0) \cdot \int_D \nabla_{\mathbf{r}'}^\perp \mathbf{v} \left(\frac{\mathbf{r}' - \mathbf{r}_0}{\epsilon}, t \right) \nabla_{\mathbf{r}'} \Phi(\mathbf{r} - \mathbf{r}') d\mathbf{r}' \\ &\quad + \eta(t) \nabla u(\mathbf{r}_0, 0) \cdot \\ &\quad \int_D \int_D \nabla_{\tilde{\mathbf{r}}} \frac{\partial}{\partial t} \left[\eta(t) \mathbf{v} \left(\frac{\tilde{\mathbf{r}} - \mathbf{r}_0}{\epsilon}, t \right) \right] \nabla_{\mathbf{r}'}^\perp \nabla_{\tilde{\mathbf{r}}} \Phi(\mathbf{r} - \mathbf{r}') \nabla_{\mathbf{r}'} \Phi(\mathbf{r} - \mathbf{r}') d\tilde{\mathbf{r}} d\mathbf{r}'. \end{aligned} \quad (3.16)$$

Next, we estimate $\sum_{j=1}^3 \mathcal{R}_j(\mathbf{r}, t)$. For \mathcal{R}_1 , we have

$$\begin{aligned} \left| \nabla_{\mathbf{r}'}^\perp \int_D \nabla_{\tilde{\mathbf{r}}} \Phi(\mathbf{r}' - \tilde{\mathbf{r}}) \cdot \nabla^\perp u(\tilde{\mathbf{r}}, t) d\tilde{\mathbf{r}} \right| &= \left| \int_D \nabla_{\mathbf{r}'}^\perp \nabla_{\tilde{\mathbf{r}}} \Phi(\mathbf{r}' - \tilde{\mathbf{r}}) \cdot \nabla^\perp u(\tilde{\mathbf{r}}, t) d\tilde{\mathbf{r}} \right| \\ &\leq \frac{3}{8\pi L^3} \int_D |\nabla^\perp u(\tilde{\mathbf{r}}, t)| d\tilde{\mathbf{r}} \leq \frac{3|\widehat{D}|^{1/2} \epsilon^{3/2}}{8\pi L^3} \|\nabla^\perp u(\cdot, t)\|_{L^2(D)} \quad \text{for } \mathbf{r}' \in \partial\Omega. \end{aligned} \quad (3.17)$$

Here, the last inequality comes from Jensen's inequality and the fact that $|D| = \epsilon^3 |\widehat{D}|$. From Lemma 1 in [6], there exists a constant $C_1 > 0$, independent of ϵ , such that

$$\begin{aligned} \|\nabla^\perp u(\cdot, t)\|_{L^2(D)} &\leq \|\nabla^\perp u(\cdot, 0)\|_{L^2(D)} + \|\nabla^\perp [u(\cdot, t) - u(\cdot, 0)]\|_{L^2(D)} \\ &\leq [\sup_{\mathbf{r} \in \widehat{D}} |\nabla^\perp u(\mathbf{r}, 0)| + C_1] |\widehat{D}|^{1/2} \epsilon^{3/2} \\ &\leq [C_2 \|g\|_{L^2(\partial\Omega)} + C_1] |\widehat{D}|^{1/2} \epsilon^{3/2}, \end{aligned} \quad (3.18)$$

where C_2 is a constant independent of ϵ . The last inequality of (3.18) comes from the standard interior estimate [9]. Substituting (3.18) into (3.17), we obtain that

$$\left| \nabla_{\mathbf{r}'}^\perp \int_D \nabla_{\tilde{\mathbf{r}}} \Phi(\mathbf{r}' - \tilde{\mathbf{r}}) \cdot \nabla^\perp u(\tilde{\mathbf{r}}, t) d\tilde{\mathbf{r}} \right| \leq \frac{3|\widehat{D}|}{8\pi L^3} [C_2 \|g\|_{L^2(\partial\Omega)} + C_1] \epsilon^3 \quad \text{for } \mathbf{r}' \in \partial\Omega.$$

Hence, we have

$$|\mathcal{R}_1(\mathbf{r}, t)| \leq |\eta'(t)| \frac{3|\widehat{D}|}{8\pi L^3} [C_2 \|g\|_{L^2(\partial\Omega)} + C_1] \mathcal{S}_\Omega[1](\mathbf{r}) \epsilon^3 \quad \text{for } \mathbf{r} \in \Omega. \quad (3.19)$$

Next, we will estimate \mathcal{R}_2 . Note that $\frac{\partial u}{\partial t}$ satisfies the following equation

$$\begin{cases} \nabla \cdot \left((1 + \eta(t)\chi_D) \nabla \frac{\partial u}{\partial t} \right) = -\nabla \cdot (\eta'(t)\chi_D \nabla u) & \text{in } \Omega, \\ \nabla \frac{\partial u}{\partial t} \cdot \mathbf{n}|_{\partial\Omega} = 0. \end{cases} \quad (3.20)$$

It follows from (3.18) and (3.20) that

$$\begin{aligned} \left\| \nabla \frac{\partial u}{\partial t}(\cdot, t) \right\|_{L^2(D)} &\leq \Lambda |\eta'(t)| \|\nabla u\|_{L^2(D)} \\ &\leq \Lambda |\eta'(t)| [C_2 \|g\|_{L^2(\partial\Omega)} + C_1] |\widehat{D}|^{1/2} \epsilon^{3/2}, \end{aligned} \quad (3.21)$$

where Λ is the positive constant given in (3.1).

By repeating the arguments as in estimating \mathcal{R}_1 , we obtain

$$|\mathcal{R}_2(\mathbf{r}, t)| \leq \Lambda^2 |\eta'(t)| \frac{3|\widehat{D}|}{8\pi L^3} [C_2 \|g\|_{L^2(\partial\Omega)} + C_1] \mathcal{S}_\Omega[1](\mathbf{r}) \epsilon^3 \quad \text{for } \mathbf{r} \in \Omega. \quad (3.22)$$

It remains to estimate \mathcal{R}_3 . From the outer expansion in [3], we have

$$u(\mathbf{r}, t) = u(\mathbf{r}, 0) - \epsilon^3 \nabla u(\mathbf{r}_0, 0) \cdot \mathcal{Q}(\lambda(t), \widehat{D}) \nabla \mathcal{N}(\mathbf{r}, \mathbf{r}_0) + O(\epsilon^4) \quad \text{for } \mathbf{r} \in \partial\Omega,$$

where $\mathcal{Q}(\lambda, \widehat{D}) = (q_{ij})_{i,j=1}^d$ is the polarization tensor given by

$$q_{ij} = \int_{\partial\widehat{D}} (\lambda(t)I - \mathcal{K}_D^*)^{-1} [\mathbf{n}_i](\xi) \xi_j d\sigma_\xi,$$

with $\lambda(t) = \frac{\eta(t)+2}{2\eta(t)}$ and $\mathcal{K}_D^* \phi(\mathbf{r}) = \int_{\partial\widehat{D}} \frac{\langle \mathbf{r}' - \mathbf{r}, \mathbf{n}_{\mathbf{r}'} \rangle}{4\pi |\mathbf{r}' - \mathbf{r}|^3} \phi(\mathbf{r}') dS_{\mathbf{r}'}$, the dual of the trace operator [8] and \mathcal{N} is the Neumann function, the solution of

$$\begin{cases} \Delta \mathcal{N}(\mathbf{r}, \mathbf{r}') = \delta(\mathbf{r} - \mathbf{r}') & \text{for } \mathbf{r} \in \Omega, \\ \frac{\partial \mathcal{N}}{\partial \mathbf{n}_{\mathbf{r}}} |_{\partial\Omega} = -\frac{1}{|\partial\Omega|}, \\ \int_{\partial\Omega} \mathcal{N}(\mathbf{r}, \mathbf{r}') dS_{\mathbf{r}'} = 0 & \text{for } \mathbf{r} \in \Omega, \end{cases} \quad (3.23)$$

Hence, we have

$$|\mathcal{R}_3(\mathbf{r}, t)| = \left| \mathcal{S}_\Omega \left[\nabla^\perp \mathcal{D}_\Omega \left[\nabla u(\mathbf{r}_0, 0) \cdot \frac{\partial \mathcal{Q}}{\partial t}(\lambda(t), \widehat{D}) \nabla \mathcal{N}(\mathbf{r}, \mathbf{r}_0) \right] \cdot \mathbf{n} \right] \right| \epsilon^3 + O(\epsilon^4). \quad (3.24)$$

Therefore, the proof of (i) follows from (3.16), (3.19), (3.22) and (3.24) with the change of variable $\xi = \frac{\mathbf{r} - \mathbf{r}_0}{\epsilon}$.

(ii) Let $\mathbf{r} \in \Omega \setminus D_d$. Using Jensen's inequality, we have

$$|\mathcal{I}_1(\mathbf{r}, t)| \leq |\eta'(t)| \frac{1}{4\pi d^2} \|\nabla^\perp u(\cdot, t)\|_{L^1(D)} \leq |\eta'(t)| \frac{|D|^{1/2}}{4\pi d^2} \|\nabla^\perp u(\cdot, t)\|_{L^2(D)}.$$

From (3.18), we obtain

$$|\mathcal{I}_1(\mathbf{r}, t)| \leq |\eta'(t)| \frac{|\widehat{D}|}{4\pi d^2} [C_2 \|g\|_{L^2(\partial\Omega)} + C_1] \epsilon^3. \quad (3.25)$$

From Calderon-Zygmund estimate [11], we have

$$\left(\int_D \left| \nabla_{\mathbf{r}'}^\perp \int_D \nabla_{\mathbf{r}} \Phi(\mathbf{r}' - \mathbf{r}) \cdot \nabla u(\mathbf{r}, t) d\mathbf{r} \right|^2 d\mathbf{r}' \right)^{1/2} \leq C_3 \|\nabla u(\cdot, t)\|_{L^2(D)},$$

where C_3 is a constant independent of ϵ . Hence, for $\mathbf{r} \in \Omega \setminus D_d$, we have

$$|\mathcal{I}_2(\mathbf{r}, t)| \leq |\eta(t)| |\eta'(t)| \frac{C_3 |\widehat{D}|}{4\pi d^2} [C_2 \|g\|_{L^2(\partial\Omega)} + C_1] \epsilon^3. \quad (3.26)$$

Same method can be used to estimate $\mathcal{I}_3(\mathbf{r}, t)$ for $\mathbf{r} \in \Omega \setminus D_d$:

$$|\mathcal{I}_3(\mathbf{r}, t)| \leq \eta^2(t) |\eta'(t)| \frac{C_3 \Lambda |\widehat{D}|}{4\pi [d + \text{dist}(\mathbf{r}, D_d)]^2} [C_2 \|g\|_{L^2(\partial\Omega)} + C_1] \epsilon^3. \quad (3.27)$$

The proof of (ii) follows from (3.25), (3.26), (3.27), (3.19), (3.22) and (3.24). This completes the proof. \square

Now we are ready to prove Theorem 3.1.

Proof of Theorem 3.1 Dividing $i\gamma T_c \mathcal{M}^1(\mathbf{r}, 0)$ on both sides of (3.3), we obtain

$$\mathcal{B}^N(\mathbf{r}, t) = \frac{1}{i\gamma T_c} \sum_{j=0}^{N-1} \frac{\mathcal{M}^1(\mathbf{r} + \mathbf{a}_j, t)}{\mathcal{M}^1(\mathbf{r}, 0)} \frac{\partial B_z}{\partial t}(\mathbf{r} + \mathbf{a}_j, t), \quad (3.28)$$

where $\mathbf{a}_j = (0, \frac{j}{N}, 0)$ for $j = 0, 1, 2, \dots, N-1$.

(i) For $\mathbf{r} \in D_{z_0}^N$, due to the periodic structure, there exists n such that $\mathbf{r}_\# \in D_{z_0}$ and $\mathbf{r} + \mathbf{a}_j \in \Omega_{z_0} \setminus (D_d \cap \{z = z_0\})$ for $j = 0, 1, 2, \dots, N-1$ and $j \neq n$. Hence, from (3.28) we obtain

$$\mathcal{B}^N(\mathbf{r}, t) = \frac{\mathcal{M}^1(\mathbf{r}_\#, t)}{i\gamma T_c \mathcal{M}^1(\mathbf{r}, 0)} \frac{\partial B_z}{\partial t}(\mathbf{r}_\#, t) + \sum_{j=0, j \neq n}^{N-1} \frac{\mathcal{M}^1(\mathbf{r} + \mathbf{a}_j, t)}{i\gamma T_c \mathcal{M}^1(\mathbf{r}, 0)} \frac{\partial B_z}{\partial t}(\mathbf{r} + \mathbf{a}_j, t). \quad (3.29)$$

(3.7) follows from the identity (3.29) and Lemma 3.2.

(ii) Let $\mathbf{r} \in (\Omega \setminus D_d) \cap \{z = z_0\}$, using the periodic structure and the assumption that $d < \frac{FOV}{3N}$, we have $\mathbf{r} + \mathbf{a}_j \in (\Omega \setminus D_d) \cap \{z = z_0\}$ for $j = 0, 1, 2, \dots, N-1$. (3.8) follows from the identity (3.28), Lemma 3.2 and the assumption (3.2). This completes the proof. \square

3.2. A remark on Theorem 3.1. According to Theorem 3.1, the N -folded $D_{z_0}^N$ can be detected from the method of thresholding:

$$D_{z_0}^N \approx \{ \mathbf{r} \in \Omega_{z_0} : |\mathcal{B}^N(\mathbf{r}, t)| \geq \Upsilon_t \}, \quad (3.30)$$

where Υ_t is a suitably chosen threshold. Although the theoretical results are obtained under the assumption that the reference conductivity is homogeneous and D is a single anomaly, various numerical simulations show that the proposed detection method works well for very general cases. In Figure 3.1, we test the proposed method when the reference conductivity $\sigma(\mathbf{r}, 0)$ is inhomogeneous and D consists of two subdomains D_1 and D_2 . We set $\Upsilon_t = 10\% \times \|\mathcal{B}^4(\cdot, t)\|_{L^\infty(\Omega_{z_0})}$. Comparing Figure 3.1 (b) and (d), we know that this approach for detecting the $D_{z_0}^4$ works very well even for the general cases.

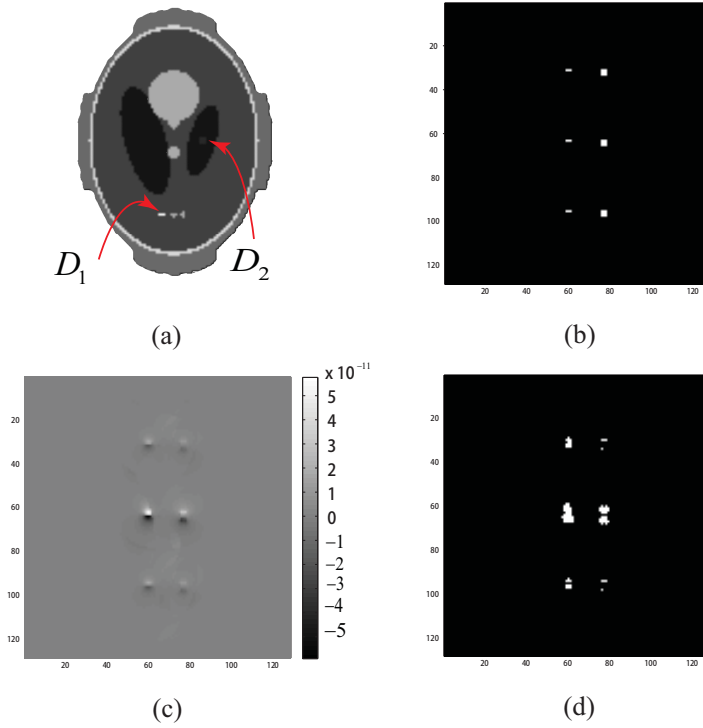


FIG. 3.1. Detection of $D_{z_0}^4$ when the reference conductivity $\sigma(\mathbf{r}, 0)$ is inhomogeneous and D consists of two subdomains D_1 and D_2 . (a) The reference conductivity distribution and configuration of two subdomains D_1 and D_2 . (b) Configuration of $D_{z_0}^4$. (c) The image of \mathcal{B}^4 . (d) The threshold image of \mathcal{B}^4 by setting $\Upsilon_t = 10\% \times \|\mathcal{B}^4(\cdot, t)\|_{L^\infty(\Omega_{z_0})}$.

3.3. Localization of D_{z_0} from \mathcal{M}^N in general case. From the arguments in the previous sections, the folded domain $D_{z_0}^N$ can be estimated from (3.30). It remains to select D_{z_0} out of $D_{z_0}^N$. The selection is possible with the use of the governing equations (2.3), (2.4), and (3.3).

To be precise, denote

$$D_{z_0}^{N,j} = \{ \mathbf{r} \in D_{z_0}^N : \mathbf{r} + (0, \frac{j}{N}, 0) \in D_{z_0} \} \quad \text{for } j = 0, 1, \dots, N-1. \quad (3.31)$$

Set $\sigma_j(x, y, z_0, t) = \sigma(x, y, z_0, 0) + \eta(t)\chi_{D_{z_0}^{N,j}}$. Using the method in [23], we generate the simulated \mathcal{M}_j^N from the formula (2.2) with the conductivity σ_j . We select a number \tilde{j} out of the set $\{0, 1, \dots, N-1\}$ which minimizes the misfit $\|\mathcal{M}^N(\cdot, t) - \mathcal{M}_j^N(\cdot, t)\|_{L^2(\Omega_{z_0})}$. Then $D_{z_0} \approx D_{z_0}^{N,\tilde{j}}$.

We summarize the selection procedures as follows:

- Step 1.* At $t = 0$, we get the data of $\mathcal{M}^1(\mathbf{r}, 0)$ and $B_z^j(\mathbf{r}, 0)$ ($j = 1, 2$) on the slice Ω_{z_0} , and reconstruct $\sigma(\mathbf{r}, 0)$ for $\mathbf{r} \in \Omega_{z_0}$ by using the harmonic B_z algorithm [18].
- Step 2.* Fix $N \geq 2$, and get the corresponding skipped k-space data for $t > 0$. Generate $\mathcal{M}^N(\mathbf{r}, t)$ by taking inverse Fourier transform.
- Step 3.* Compute $\mathcal{B}^N(x, y, z_0, t)$ in (3.4).
- Step 4.* For a given threshold Υ_t , segment the N -folded region $D_{z_0}^N$ by (3.30).
- Step 5.* For each $D_{z_0}^{N,j}$, $j = 0, 1, 2, \dots, N-1$, set $\sigma_j(\mathbf{r}, t) = \sigma(\mathbf{r}, 0) + \eta(t)\chi_{D_{z_0}^{N,j}}$ to generate the simulated data \mathcal{M}_j^N .
- Step 6.* Select $\tilde{j} = \arg \min_{j \in \{0, 1, \dots, N-1\}} \|\mathcal{M}^N(\cdot, t) - \mathcal{M}_j^N(\cdot, t)\|_{L^2(\Omega_{z_0})}$ and $D_{z_0} = D_{z_0}^{N,\tilde{j}}$.

4. Numerical experiments. To validate the proposed algorithm, we perform numerical experiments by constructing a modified 3D Shepp and Logan phantom [24]. This phantom is constructed by 11 ellipsoids using COMSOL 3.5a. Figure 4.1 (a) illustrates the geometry of this phantom. In Figure 4.1 (b), we cut a half of the out layers of this phantom to see the internal structures. There are two subdomains D_j ($j = 1, 2$) where the conductivity changes occur; in Figure 3.1 (a) we show the position of D_j through a slice Ω_{z_0} of Ω . We assume that $\sigma(\mathbf{r}, t) = \sigma(\mathbf{r}, 0) + 0.04t\chi_{D_1} + 0.02t\chi_{D_2}$, where $\sigma(x, y, z_0, 0)$ is illustrated in Figure 4.1 (c). Two pairs of electrodes \mathcal{E}_j^\pm ($j = 1, 2$) are attached to $\partial\Omega$. Through \mathcal{E}_j^\pm we inject a sinusoidal current with amplitude of 5mA (see Figure 2.1). The z -th component of the magnetic flux density \mathbf{B} , B_z , can

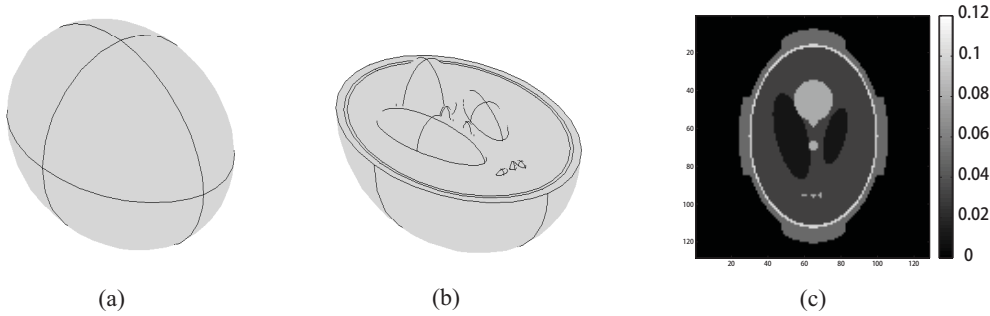


FIG. 4.1. Modified 3D Shepp and Logan phantom; (a) geometry of the phantom; (b) the internal structures of the phantom; (c) conductivity distribution in the cross-sectional slice Ω_{z_0} at $t = 0$.

be generated using the forward solver proposed in [12, 21]. Particularly, for $t = 0$, we inject two linearly independent current I_j through two pairs of surface electrodes \mathcal{E}_j^\pm . The generated $B_z^j(x, y, z_0, 0)$ ($j = 1, 2$) are respectively shown in Figure 4.2 (a) and (b). Using the harmonic B_z algorithm [18], we reconstruct the reference conductivity distribution $\sigma(x, y, z_0, 0)$; the reconstruction result is shown in Figure 4.2 (c).

For $t > 0$, we first generate the k-space signal $S(k_x, k_y, z_0, t)$ by taking Fourier transform of $\mathcal{M}^1(x, y, z_0, t)$ which can be calculated from formula (2.2). We skip

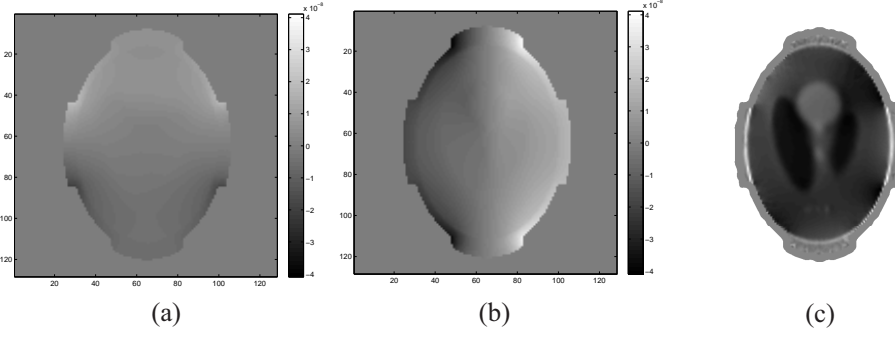


FIG. 4.2. Reconstruction of the reference conductivity using harmonic B_z algorithm: (a) the image of $B_z^1(x, y, z_0, 0)$; (b) the image of $B_z^2(x, y, z_0, 0)$; (c) the reconstructed conductivity distribution $\sigma(x, y, z_0, 0)$.

$S(k_x, k_y, z_0, t)$ by N steps in the y direction, and generate $S^N(k_x, k_y, z_0, t)$. Figure 4.3 illustrates the fully sampled k-space data $S^1(k_x, k_y, z_0, 0)$ and undersampled k-space data for $S^N(k_x, k_y, z_0, 1)$ by a factor of $N = 4$. If we take inverse Fourier

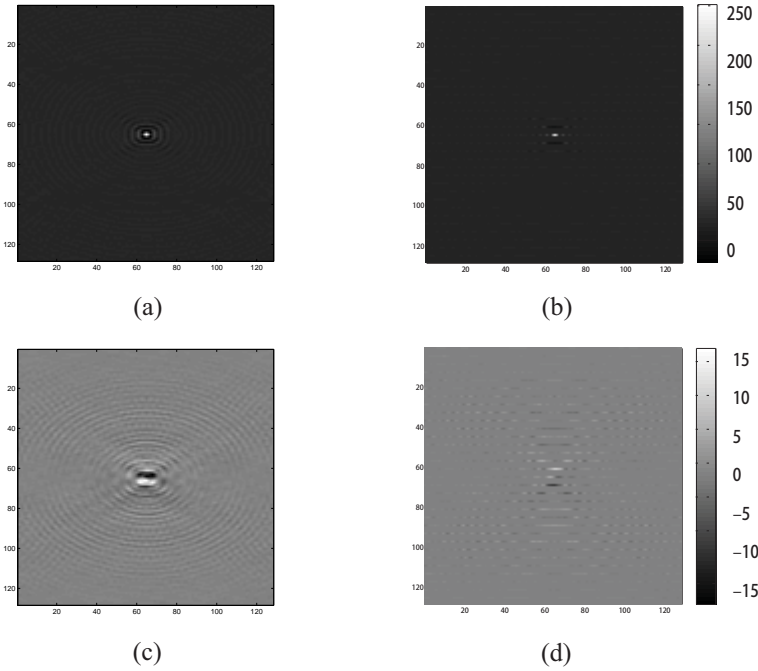


FIG. 4.3. MR k-space data: (a) and (c) show the real and imaginary parts of $S^1(k_x, k_y, z_0, 0)$ respectively; (b) and (d) show the real and imaginary parts of $S^4(k_x, k_y, z_0, 1)$.

transform of $S^4(k_x, k_y, z_0, 1)$, we will obtain the 4-folded complex magnitude image $\mathcal{M}^4(x, y, z_0, 1)$ shown in Figure 4.4. Using these images and the formula (3.4), \mathcal{B}^4 can be obtained in Figure 4.5 (a). By setting $\Upsilon_1 = 10\% \times \|\mathcal{B}^4(\cdot, 1)\|_{L^\infty(\Omega_{z_0})}$, we could get the threshold results shown in Figure 4.5 (b).

To select the domain D_{z_0} from the 4-folded $D_{z_0}^4$, we need to minimize the misfit function $\|\mathcal{M}_{j_1, j_2}^4(\cdot, 1) - \mathcal{M}^4(\cdot, 1)\|_{L^2(\Omega_{z_0})}$. The meaning of j_1 and j_2 are depicted

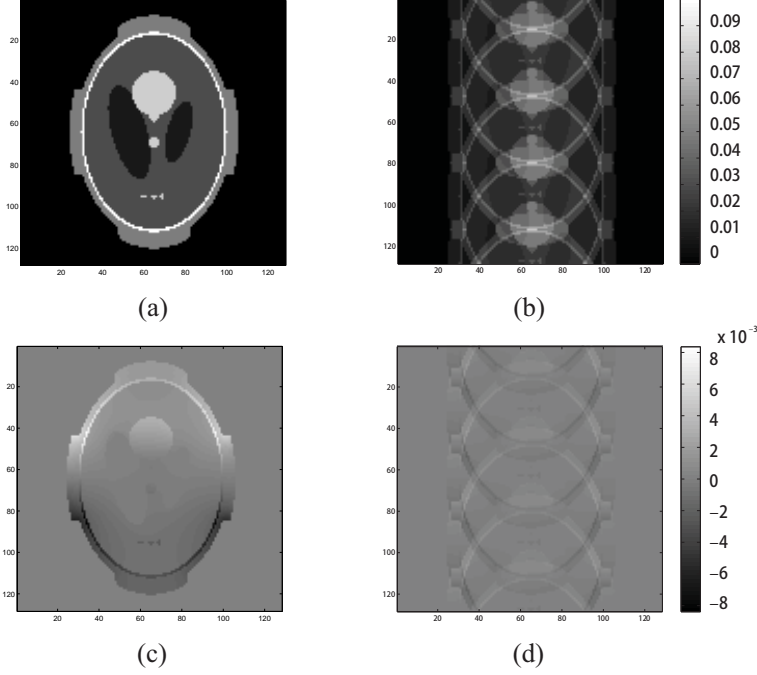


FIG. 4.4. MR images: (a) and (c) show the real and imaginary parts of $\mathcal{M}^1(k_x, k_y, z_0, 0)$; (b) and (d) show the real and imaginary parts of $\mathcal{M}^4(k_x, k_y, z_0, 1)$.

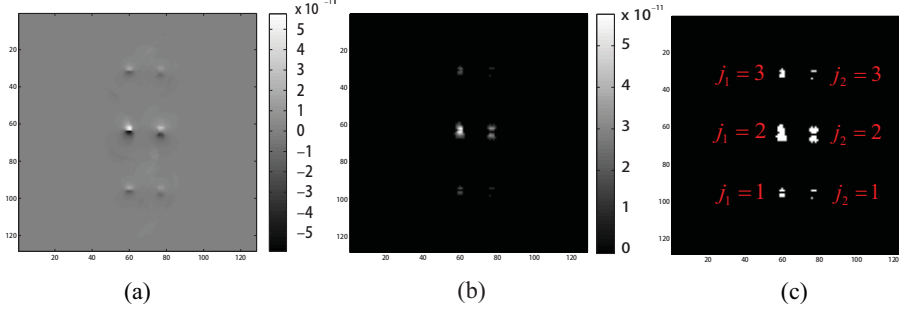


FIG. 4.5. (a) is the image of $\mathcal{B}^4(x, y, z_0, 1)$. (b) is the threshold result by setting $\Upsilon_1 = 10\% \times \|\mathcal{B}^4(\cdot, 1)\|_{L^\infty(\Omega_{z_0})}$. (c) shows the meaning of j_1 and j_2 in the notation \mathcal{M}_{j_1, j_2}^4 .

in Figure 4.5 (c). Table 4.1 gives the results of $\|\mathcal{M}_{j_1, j_2}^4(\cdot, 1) - \mathcal{M}^4(\cdot, 1)\|_{L^2(\Omega_{z_0})}$ for $j_1, j_2 = 1, 2, 3$. As we can see that when $j_1 = 1, j_2 = 2$, $\|\mathcal{M}_{j_1, j_2}^4(\cdot, 1) - \mathcal{M}^4(\cdot, 1)\|_{L^2(\Omega_{z_0})}$ is minimized. Therefore, $D_{z_0} = D_{z_0}^{4,1,2}$.

To test the performance of our algorithm, we also set $N = 8, N = 16$ and $N = 32$; for these N , Figure 4.6 illustrates the images of $\mathcal{B}^N(x, y, z_0, 1)$ and the threshold results by setting $\Upsilon_1 = 10\% \times \|\mathcal{B}^N(\cdot, 1)\|_{L^\infty(\Omega_{z_0})}$. As we can see from the images that, it is possible to localize the source region D_{z_0} if $N = 8$ and $N = 16$. However, since each $D_{z_0}^{N,j}$ is not well separated, it could be difficult to localize D_{z_0} for the case $N = 32$.

At last, we add Gaussian random noise to the simulated B_z . From [13, 17] we

TABLE 4.1
 Values of $\|\mathcal{M}_{j_1, j_2}^4(\cdot, 1) - \mathcal{M}^4(\cdot, 1)\|_{L^2(\Omega_{z_0})}$ for $SNR = \infty$

	$j_1 = 1$	$j_1 = 2$	$j_1 = 3$
$j_2 = 1$	1.356×10^{-7}	1.669×10^{-7}	1.659×10^{-7}
$j_2 = 2$	0	1.604×10^{-7}	1.525×10^{-7}
$j_2 = 3$	1.176×10^{-7}	1.608×10^{-7}	1.527×10^{-7}

know that the standard deviation s of B_z is given by $s = 1/2\gamma T_c SNR$, where $T_c = 50$ ms and $SNR = 2000$ is the signal-to-noise ratio. Repeating the above procedures, we get the images of $\mathcal{B}^N(x, y, z_0, 1)$ for $N = 4, 8, 16$ as shown in Figure 4.7. Table 4.2 gives the values of $\|\mathcal{M}_{j_1, j_2}^4(\cdot, 1) - \mathcal{M}^4(\cdot, 1)\|_{L^2(\Omega_{z_0})}$ for $SNR = 2000$. From Table 4.2, it is obvious that $D_{z_0} = D_{z_0}^{4,1,2}$.

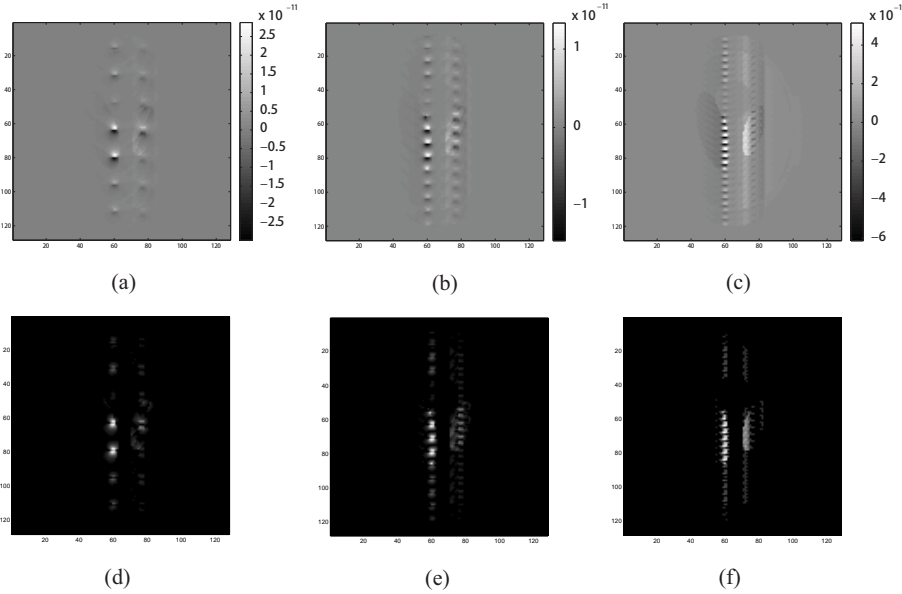


FIG. 4.6. Images of $\mathcal{B}^N(x, y, z_0, 1)$ and the threshold images for $SNR = \infty$. (a), (b) and (c) are respectively images of $\mathcal{B}^N(x, y, z_0, 1)$ for $N = 8, 16$ and 32 . (d), (e) and (f) are respectively the corresponding threshold results for $\Upsilon_1 = 10\% \times \|\mathcal{B}^N(\cdot, 1)\|_{L^\infty(\Omega_{z_0})}$.

TABLE 4.2
 Values of $\|\mathcal{M}_{j_1, j_2}^4(\cdot, t) - \mathcal{M}^4(\cdot, t)\|_{L^2(\Omega_{z_0})}$ for $SNR = 2000$

	$j_1 = 1$	$j_1 = 2$	$j_1 = 3$
$j_2 = 1$	8.92×10^{-7}	8.991×10^{-7}	8.978×10^{-7}
$j_2 = 2$	8.795×10^{-7}	8.940×10^{-7}	8.922×10^{-7}
$j_2 = 3$	8.862×10^{-7}	8.952×10^{-7}	8.942×10^{-7}

5. Discussion and conclusion. In this paper, we provide a mathematical ground for highly undersampled MREIT, which aims to localize conductivity changes

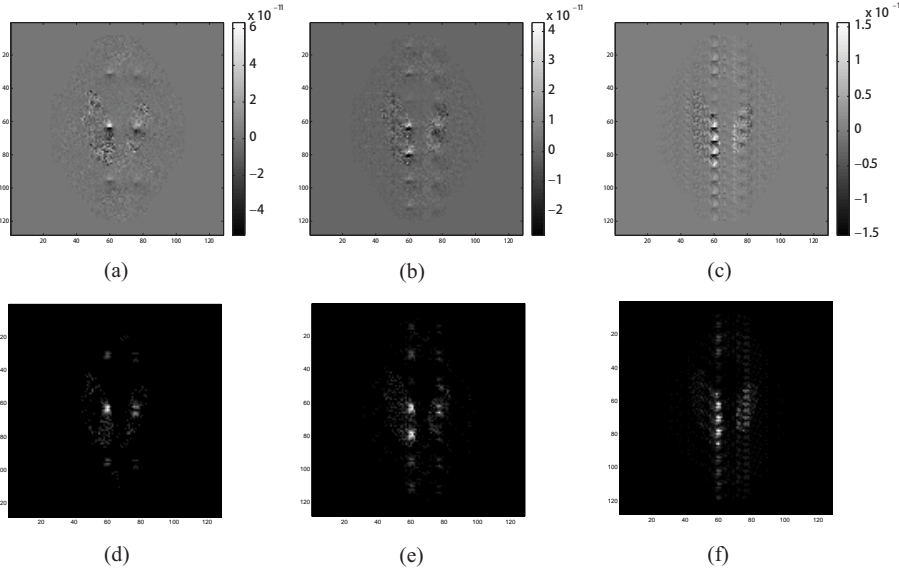


FIG. 4.7. Images of $\mathcal{B}^N(x, y, z_0, 1)$ and the threshold images for $SNR=2000$ and $N=4, 8$ and 16. Each figure has the similar meaning as that in Figure 4.6.

associated with tissue physiological activity. Numerical simulations show that the proposed method is capable of localizing the conductivity changes using only 1/16 of the k-space data. Since the data acquisition speed is roughly proportional to the number of the phase encoding encoding lines in the k-space, 1/ N -subsamped MREIT may has nearly N times faster data acquisition speed. Hence, the proposed method can be used for functional MREIT to provide a mapping of conductivity perturbation associated with neural activity or pathological changes in tissue [14, 27]. Future studies include in vivo animal experiments to test the performance of the proposed method in practical environment.

REFERENCES

- [1] H. AMMARI, S. MOSKOW, AND M.S. VOGELIUS, *Boundary integral formulae for the reconstruction of electric and electromagnetic inhomogeneities of small volume*, ESAIM Control Optim. Calc. Var. 9 (2003), pp. 49–66.
- [2] H. AMMARI AND A. KHELIFI, *Electromagnetic scattering by small dielectric inhomogeneities*, J. Math. Pures Appl. 82 (2003), pp. 749–842.
- [3] H. AMMARI, J. GARNIER, W. JING, H. KANG, M. LIM, K. SØLNA AND H. WANG, *Mathematical and Statistical Methods for Multistatic Imaging*, Lecture Notes in Mathematics, Springer-Verlag, Switzerland, 2013.
- [4] K. Y. ARISTOVICH, G. S. SANTOS, B. C. PACKHAM AND D. S. HOLDER, *A method for reconstructing tomographic images of evoked neural activity with electrical impedance tomography using intracranial planar arrays*, Physiol. Meas. 35 (2014), pp. 1095–1109.
- [5] J. BODURKA AND P. A. BANDETTINI *Toward direct mapping of neuronal activity: MRI detection of ultraweak, transient magnetic field changes*, Magn. Reson. Med. 47 (2002), pp. 1052–1058.
- [6] D. J. CEDIO-FENGYA, S. MOSKOW, AND M. S. VOGELIUS, *Identification of conductivity imperfections of small diameter by boundary measurements. Continuous dependence and computational reconstruction*, Inverse Problems, 14 (1998), pp. 553–595.
- [7] Z. ELAZAR, R. T. KADO AND W. R. ADEY *Impedance changes during epileptic seizures* *Epilepsia*, 7(1966), pp. 291–307.

- [8] G. B. FOLLAND AND B. GERALD, *Introduction to partial differential equations*, Princeton University Press, Princeton, NJ, 1995. Reprint of the 1998 edition.
- [9] D. GILBARG AND N. S. TRUDINGER, *Elliptic partial differential equations of second order*, Classics in Mathematics, Springer-Verlag, Berlin, 2001. Second edition.
- [10] K. A. KLIVINGTON AND R. GALAMBOS, *Resistance shifts accompanying the evoked cortical response in the cat*, Science, 157(1967), pp. 211-213.
- [11] O. KWON, AND J. K. SEO, *Total size estimation and identification of multiple anomalies in the inverse conductivity problem*, Inverse Problems, 17 (2001), pp. 59-75.
- [12] B. O. LEE, S. H. OH, E. J. WOO, S. Y. LEE, M. H. CHO, O. KWON, J. K. SEO, J. Y. LEE AND W. S. BAEK, *Three-dimensional forward solver and its performance analysis in Magnetic Resonance Electrical Impedance Tomography (MREIT) using recessed electrodes*, Phys. Med. Biol. 48 (2003), pp. 1971-1986.
- [13] R. SADLEIR, S. GRANT, S. U. ZHANG, B. I. LEE, H. C. PYO, S. H. OH, C. PARK, E. J. WOO, S. Y. LEE, O. KWON AND J. K. SEO, *Noise analysis in MREIT at 3 and 11 Tesla field strength*, Physiol. Meas. 26(2005), pp. 875-884.
- [14] R. SADLEIR, S. GRANT, S. U. ZHANG, S. H. OH, B. I. LEE AND E. J. WOO, *High field MREIT: setup and tissue phantom imaging at 11 T*, Physiol. Meas. 27 (2006), pp. S261-S270.
- [15] G. S. SANTOS, A. N. VONGERICHTEN, K. ARISTOVICH, J. AVERY, A. MCEVOY, M. WALKER AND D. S. HOLDER, *Characterisation and imaging of cortical impedance changes during interictal and ictal activity in the anaesthetised rat* NeuroImage, 124(2015), pp. 813-823.
- [16] G. C. SCOTT, M. L. G. JOY, R. L. ARMSTRONG, AND R. M. HENKELMAN, *Measurement of nonuniform current density by magnetic resonance*, IEEE Trans. Med. Imag., 10 (1991), pp. 362-374.
- [17] G. C. SCOTT, M. L. G. JOY, R. L. ARMSTRONG AND R. M. HENKELMAN, *Sensitivity of magnetic-resonance current-density imaging*, J. Mag. Res., 97(1992), pp. 235-254.
- [18] J. K. SEO, J. R. YOON, E. J. WOO, AND O. KWON, *Reconstruction of conductivity and current density images using only one component of magnetic field measurements*, IEEE Trans. Biomed. Eng., 50 (2003), pp. 1121-1124.
- [19] J. K. SEO AND E. J. WOO, *Magnetic resonance electrical impedance tomography (MREIT)*, SIAM Rev., 53 (2011), pp. 40-68.
- [20] J. K. SEO, D. H. KIM, J. LEE, O. I. KWON, S. Z. K. SAJIB AND E. J. WOO, *Electrical tissue property imaging using MRI at dc and Larmor frequency*, Inverse Problems, 28(2012), 26pp.
- [21] J. K. SEO, AND E. J. WOO, *Nonlinear inverse problems in imaging*, John Wiley & Sons, 2012.
- [22] J. K. SEO, AND E. J. WOO, *Electrical tissue property imaging at low frequency using MREIT*, IEEE Trans. Biomed. Eng., 61 (2014), pp. 1390-1399.
- [23] J. K. SEO, E. J. WOO, U. KATSCHER, AND Y. WANG, *Electro-Magnetic Tissue Properties MRI*, World Scientific Publishing Company, 2014.
- [24] L. A. SHEPP, AND B. F. LOGAN *The Fourier reconstruction of a head section*, IEEE Trans. Nucl. Sci., 21 (1974), pp. 21-43.
- [25] R. VELLUTI, K. KLIVINGTON AND R. GALAMBOS, *Evoked resistance shifts in subcortical nuclei*, Biosystems, 2(1968), pp. 78-80.
- [26] E. J. WOO AND J. K. SEO, *Magnetic resonance electrical impedance tomography (MREIT) for high-resolution conductivity imaging*, Physiol. Meas., 29 (2008), pp. R1-R26.
- [27] E. J. WOO, *Functional Brain Imaging using MREIT and EIT: Requirements and Feasibility*, NFSI & ICBEM, Conf. Proc. IEEE Eng. Med. Biol. Soc., (2011), pp. 7025-7028.